Clin Neuroradiol (2015) 25:109–125
DOI 10.1007/s00062-014-0360-0

REVIEW ARTICLE

Cavernous Sinus: A Comprehensive Review of its Anatomy, Pathologic Conditions, and Imaging Features

A.A. Bakan · A. Alkan · S. Kurtcan · A. Aralaşmak · S. Tokdemir · E. Mehdi · H. Özdemir

Received: 1 October 2014 / Accepted: 7 November 2014 / Published online: 20 November 2014

Abstract The purpose of this article was to review the anatomy of the cavernous sinus (CS), illustrate numerous lesions that can affect the CS, and emphasize the imaging characteristics for each lesion to further refine the differential diagnoses. The CS, notwithstanding its small size, contains a complicated and crucial network that consists of the carotid artery, the venous plexus, and cranial nerves. The wide-ranging types of pathologies that can involve the CS can be roughly classified as tumoral, congenital, infectious/inflammatory/granulomatous, and vascular. Conditions that affect the CS usually lead to symptoms that are similar to each other; thus, for diagnosis, imaging procedures are required. Radiological evaluations are also required to detect pre- and postoperative CS invasion. Magnetic resonance imaging, which can be supplemented with thin-section contrast-enhanced sequences, is the preferred imaging technique for evaluating the CS. For correct diagnosis of CS lesions and accurate evaluations of CS invasions, it is essential to carefully analyze the anatomical structures within the CS and to acquire precise knowledge about the imaging features of CS lesions, which may frequently overlap.

Keywords Cavernous sinus · Imaging · Brain · Anatomy · Pathologies

A.A. Bakan, MD (✉) · A. Alkan · S. Kurtcan, MD · A. Aralaşmak · S. Tokdemir, MD · E. Mehdi, MD · H. Özdemir
Department of Radiology, Faculty of Medicine, Bezmialem Vakif University,
34093 Fatih, Istanbul, Turkey
e-mail: ahsen80@hotmail.com

Introduction

The cavernous sinus (CS), which is a critical region in the skull base, contains a complex mixture of the cranial nerves (CNs) III, IV, V_1, V_2, and VI, the internal carotid artery (ICA), and the venous plexus. These structures, which can be encased or invaded by neoplastic, inflammatory, or vascular lesions, are usually accompanied by multiple cranial neuropathies. Magnetic resonance (MR) imaging, which can be supplemented with thin-section contrast-enhanced sequences, is the preferred imaging technique for evaluating the CS. Although primary conditions of the CS and conditions that involve the CS are relatively rare, it is critical to accurately detect these diseases with MR imaging due to the important connections of this small space. The types of CS lesions and their relationships to the structures lying within the CS play a key role in the choice of proper surgical or medical therapeutic modalities. Therefore, in this review, we focus on CS anatomy and discuss its pathological processes and their imaging characteristics to aid in the successful diagnosis of CS pathologies.

Anatomy and Imaging Protocol

The CS, which is a complex venous space, is surrounded by the meningeal and periosteal dural folds, and it is located on the lateral sides of the sella turcica. The CS extends anteriorly to the superior orbital fissure and posteriorly to the dorsum sellae and Meckel's cave.

The exterior surfaces of the CSs are confined by four dural walls: the medial, lateral, superior, and posterior walls [1]. The medial wall, which is the only wall that contains a single dural layer, has two portions: the sphenoidal and sellar portions. The sellar part of the medial wall of the CS

is the weakest area in the cover of the pituitary gland; as a result, lateral tumoral growth can occur into the CS. The other three walls consist of two dural layers: the external (meningeal dura) and the internal (periosteal dura) layers. The lateral wall contains the CNs III and IV superiorly and the CNs V_1 and V_2 inferiorly in its internal layer. While the CNs III, IV, and V_1 exit the cranium through the superior orbital fissure, the CN V_2 exits the cranium through the foramen rotundum. The superior wall, which is also called the CS roof, is formed by the carotid, clinoid, and oculomotor triangles [1]. CN III is located in the arachnoid cistern in the oculomotor triangle. The posterior wall is part of the dura that covers the clivus. The CN VI runs close to the posterior wall and enters the orbit through the superior orbital fissure. The cavernous segment of the ICA with its accompanying sympathetic neural plexus continues just medial to the CN VI. The ICA and CN VI pass through the CS sinusoids.

The CS communicates with various paracavernous venous channels. Posteroinferiorly, the CS communicates with the inferior petrosal sinus and drains into the internal jugular vein. Posterosuperiorly, it communicates with the superior petrosal sinus and drains into the transverse sinus and then into the internal jugular vein. Extracranially, it communicates with the pterygoid venous plexus to drain into the deep facial vein [2]. The two CSs are also interconnected with each other in the midline by the small anterior and posterior intercavernous sinuses and the basal venous plexus [2]. The CS receives blood from the superior and inferior ophthalmic vein, the superficial middle cerebral vein, the sphenoparietal sinus, and the inferior cerebral veins [2].

Finally, the CS is formed by the adipose and fibrous tissues that are distributed between the intracavernous vascular structures and the intracavernous CNs [3].

The CS can be comprehensively evaluated with an MR imaging protocol that includes thin-section (≤3 mm) contrast-enhanced images with fat suppression in the axial and coronal planes in addition to routine nonenhanced T1-weighted (T1W), T2-weighted (T2W), and fluid-attenuated inversion recovery sequences of the whole brain. Furthermore, contrast-enhanced three-dimensional constructive interference in steady-state T2W images may allow distinct visualization of all CNs passing through the CS and adjacent cisterns [4]. The optimal imaging protocol can include additional imaging techniques, such as vascular and orbital imaging, depending on the suspected diagnosis.

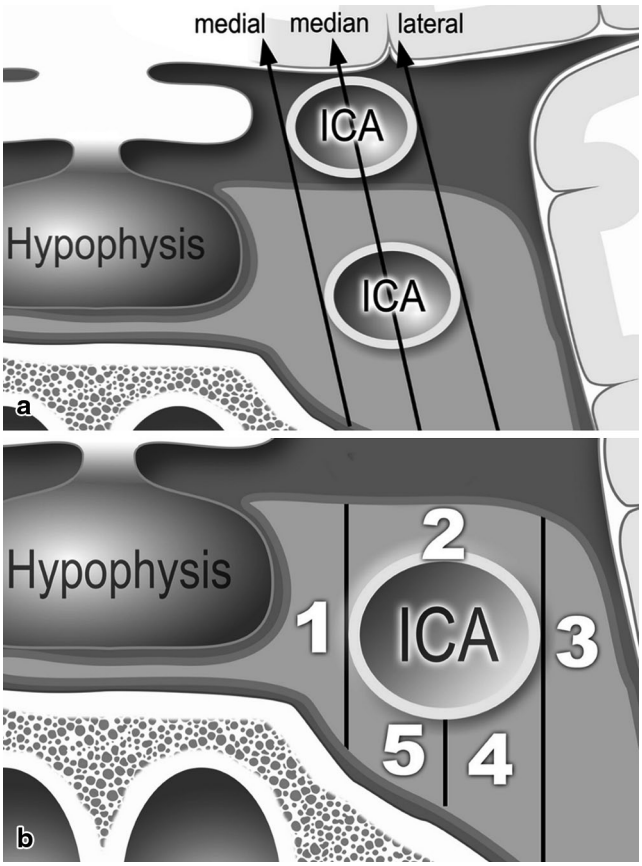

Fig. 1 **a** Diagram showing intercarotid lines. The drawing of the frontal view shows intercarotid lines between the supracavernous and intracavernous segments of the internal carotid artery (ICA): the medial intercarotid line traverses along the medial walls of the ICA, and the lateral intercarotid line traverses along the lateral walls, while the median intercarotid line traverses through the center of the ICA. **b** Diagram of the venous compartments of the cavernous sinus (CS). The drawing of the frontal view shows five venous compartments with regard to the cavernous ICA: *1* medial venous compartment, *2* superior venous compartment, *3* lateral venous compartment, *4* inferolateral venous compartment, *5* carotid sulcus venous compartment

Benign and Malignant Tumors

Pituitary Adenoma

Pituitary adenomas are benign tumors that frequently remain confined to the sella turcica or compress adjacent anatomical structures. However, approximately 6–10 % of pituitary adenomas infiltrate the CS, and these are considered more aggressive invasive neoplasms [5, 6]. Adenomas appear iso- to hypointense compared with gray matter on T1W images, and their intensity relative to the gray matter varies on T2W images [7]. On postcontrast images, adenomas appear as slowly enhancing lesions, and on early images, the relative hypointensity of the adenoma is increased compared with the adjacent gland.

Numerous studies have discussed the neuroimaging criteria for CS invasion [8–10]. Knosp et al. [8] proposed the use of the medial, median, and lateral intercarotid lines (Fig. 1a), with the ICA serving as the imaging landmark. They suggested a five-point classification system based on coronal MR imaging findings: grade 0, adenoma not encroaching the medial intercarotid line; grade 1, adenoma crossing

the medial intercarotid line but not extending beyond the median intercarotid line; grade 2, adenoma crossing the median intercarotid line but not passing beyond the lateral intercarotid line; grade 3, adenoma extending beyond the lateral intercarotid line; and grade 4, adenoma completely enclosing the ICA. According to Knosp et al., pituitary adenomas that are radiologically classified as grade 2 or higher are frequently found to have CS invasion at surgery.

In another study, Cottier et al. [9] examined detailed MR imaging indicators with respect to intraoperative findings, including the extent to which the intracavernous ICA is encased by the tumor, the grade of parasellar extension with reference to the intercarotid lines described by Knosp et al., and the invasion status of the CS venous space. To assess the latter, Cottier et al. divided the CS into five venous compartments with respect to the lCA: medial, superior, carotid sulcus, inferolateral, and lateral (Fig. 1b). Cottier et al. suggested that 67% or greater encasement of the intracavernous ICA was the most specific predictor of CS invasion. Invasion was also highly likely if the lateral intercarotid line was crossed, or if the carotid sulcus venous compartment was occluded (Figs. 2 and 3). Conversely, CS invasion was highly unlikely if less than 25% of the intracavernous ICA was encased by the tumor or if the medial intercarotid line was not crossed by the tumor.

CS invasion is the strongest prognostic factor for the presence of residual pituitary adenoma after trans-sphenoidal removal [11, 12]. Thus, detailed preoperative MR imaging assessment is crucial in surgical planning.

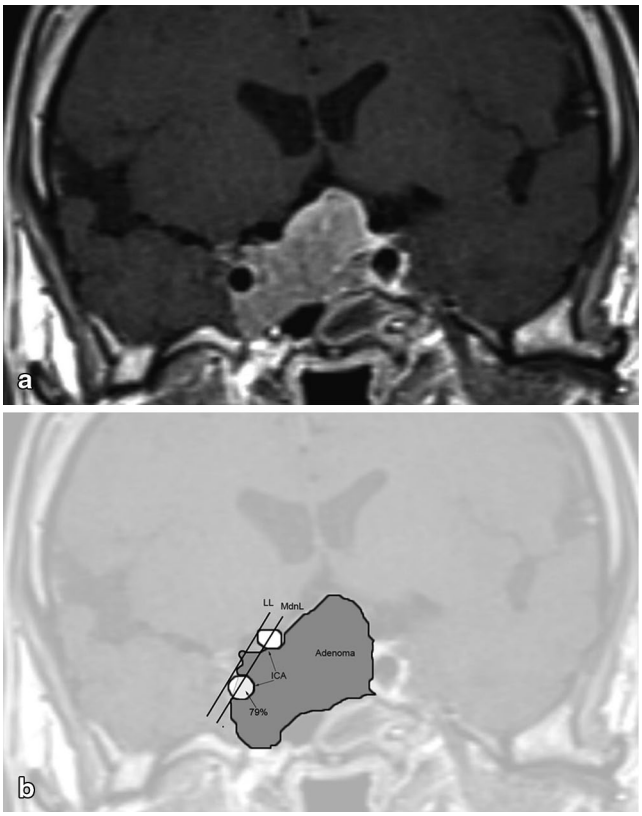

Fig. 2 Postoperative pituitary adenoma. Contrast-enhanced T1-weighted (T1W; **a**) magnetic resonance (MR) image and the corresponding drawing (**b**) show postoperative pituitary macroadenoma residue. The adenoma has an expansion toward the right CS. CSs have asymmetric size and morphology. The right cavernous ICA is approximately 79% encased; the medial, superior, inferolateral, and carotid sulcus venous compartments are obliterated; and the lateral intercarotid line is crossed (Knosp grade 3), suggesting a high likelihood of CS invasion (*LL* lateral intercarotid line, *MdnL* median intercarotid line)

Meningioma

Meningiomas, along with pituitary adenomas, are among the most common tumors that invade the CS [13], and can also occur as primary tumors in the CS [14]. They are generally iso- or hypointense on T1W and T2W images and show early homogeneous enhancement on postcontrast images (Fig. 4). CS meningiomas (CSMs) may be heterogeneous in texture owing to the presence of calcifications, cystic foci, hemorrhage, or tumor vasculature. Tumor invasion and hypervascular reaction can result in changes such as adjacent hyperostosis or dural tails. Some CSMs, especially large ones, may compress the adjacent ICA and constrict its lumen [15].

Hemangioma

CS cavernous hemangiomas (CSCHs) can originate from intracavernous components or extracavernous tissues that are adjacent to the CS [16, 17] and predominantly affect middle-aged women. Because of the tumor's propensity to bleed during resection, preoperative diagnosis is essential. CSCHs are well-defined tumors that appear iso- or hypointense on T1W images and markedly hyperintense on T2W images (Fig. 5). Following contrast administration, lesions display a peripheral to central "filling in" appearance. An important differential diagnosis of CSCHs is meningioma [18]. Prominent high signal intensity on T2W images and centripetal "filling in" contrast patterns are suggestive features that should be considered for a diagnosis of CSCH [18]. However, when imaging shows homogeneous enhancement, it is difficult to distinguish CSCHs from meningiomas or other common CS tumors.

Schwannoma

The trigeminal nerve is the most common site of origin for CS schwannomas, although they may also arise in other sensory nerves, such as the oculomotor nerve and, rarely, the abducens nerve. Tumor growth within the prepontine cistern can lead to compression of the facial, vestibulocochlear, and glossopharyngeal nerves. Schwannomas are generally well-defined solid masses, while a cystic appearance with fluid–

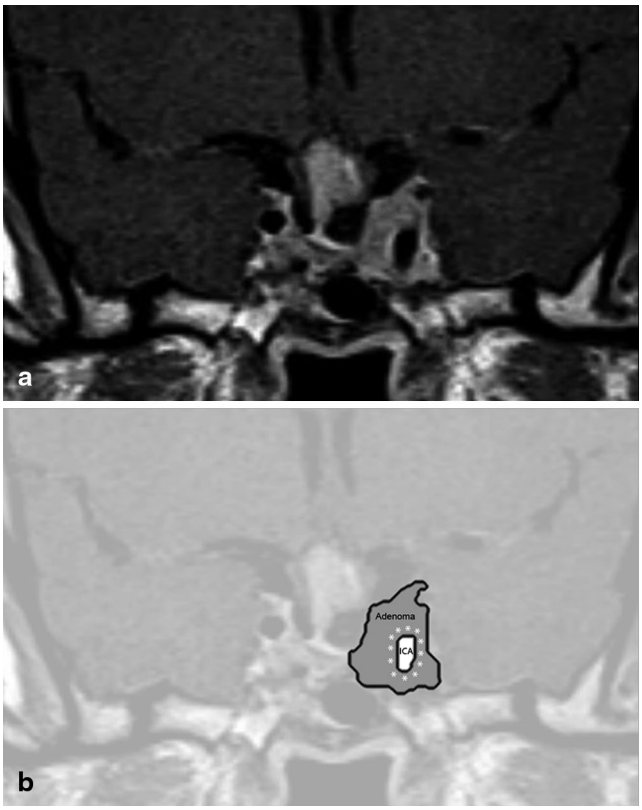

Fig. 3 Postoperative pituitary adenoma. A coronal contrast-enhanced T1W MR image (**a**) and corresponding drawing (**b**) show postoperative pituitary adenoma residue. The adenoma invades the left CS with complete encasement of the cavernous ICA (*asterisk* in **b**), and neither compartment of the CS is visible, suggesting Knosp grade 4 invasion

fluid levels is unusual. Trigeminal nerve CS schwannoma often has a characteristic dumbbell-shaped appearance with involvement of the middle and posterior fossae [19]. However, a dumbbell-shaped abducens schwannoma with extension into the CS and the prepontine area has been reported in two cases [20, 21]. Generally, small schwannomas have homogeneous signal intensities, while large schwannomas display heterogeneous signal intensities. Most schwannomas appear hypo- to isointense on T1W images and hyperintense on T2W images, while they also display moderate contrast enhancement (Fig. 6).

Plexiform Neurofibroma and Malignant Peripheral Nerve Sheath Tumor

Plexiform neurofibroma usually develops during the first 2 decades of life as a characteristic feature of neurofibromatosis 1. The tumor commonly arises in the sensory nerves, especially in the first branch of the trigeminal nerve. MR imaging scans often show diffuse enlargement and tortuous expansion of a long nerve segment into the CS [22, 23]. Plexiform neurofibroma appears hypointense on T1W images and may display homogeneous or peripheral hyperintensity with a central hypointense focus, resulting in a target sign, on T2W images. Contrast enhancement patterns are variable, ranging from mild to markedly homogeneous or heterogeneous.

Most plexiform neurofibromas are benign tumors, but approximately 10% may eventually transform into malignant peripheral nerve sheath tumors. These aggressive tumors rarely invade the CS. Follow-up radiological examinations might indicate malignant changes such as rapid growth, large tumor size, and inhomogeneous signal intensity owing to intratumoral hemorrhage and necrosis [24].

Nasopharyngeal Carcinoma

Invasion of the CS by nasopharyngeal carcinoma is common, and this involvement may be the initial presentation of a nasopharyngeal carcinoma. The most frequent extension route of nasopharyngeal carcinoma into the CS is perineural spread through the foramen ovale, and a less frequent perineural route is through the foramen lacerum [25]. Intracranial extension may also occur directly via the skull base erosion [25]. The typical MR imaging characteristics are an enlarged CS with contrast enhancement and tumor formation inside the CS. Diffuse or local dural thickening of the sinus might also be observed. A nasopharyngeal carcinoma appears hypointense on T1W and T2W images. The less aggressive types may appear mildly hyperintense on T2W images. Contrast enhancement is moderate or prominent and usually inhomogeneous (Fig. 7).

Metastases

Head and neck tumors are the most common tumors that metastasize to the CS. Distant metastases frequently originate from tumors of the breast, lung, and prostate [26]. Additionally, there are several case reports about metastases from cancers that do not typically metastasize to the CS such as thymomas and melanomas, in addition to reports on metastases from gastric, intestinal, hepatocellular, renal, testicular, and uterine carcinomas [26–28]. Metastases invade the CS by direct vascular extension or through hematogenous or perineural spread. MR imaging scans either reveal an enlargement of the CS due to a lesion or demonstrate characteristics of perineural tumor extension, including nerve bulging and enhancement, foraminal obliteration and enlargement, destruction of the foraminal fat planes, convexity of the lateral CS contour, and replacement of the trigeminal cistern with soft tissue (Fig. 8). CS metastases and nasopharyngeal carcinomas might display identical imaging results. To best differentiate them, it should be considered that a nasopharyngeal carcinoma mostly derives from the Rosen Muller fossa and then invades the CS, whereas metastatic lesions originate from the CS [29].

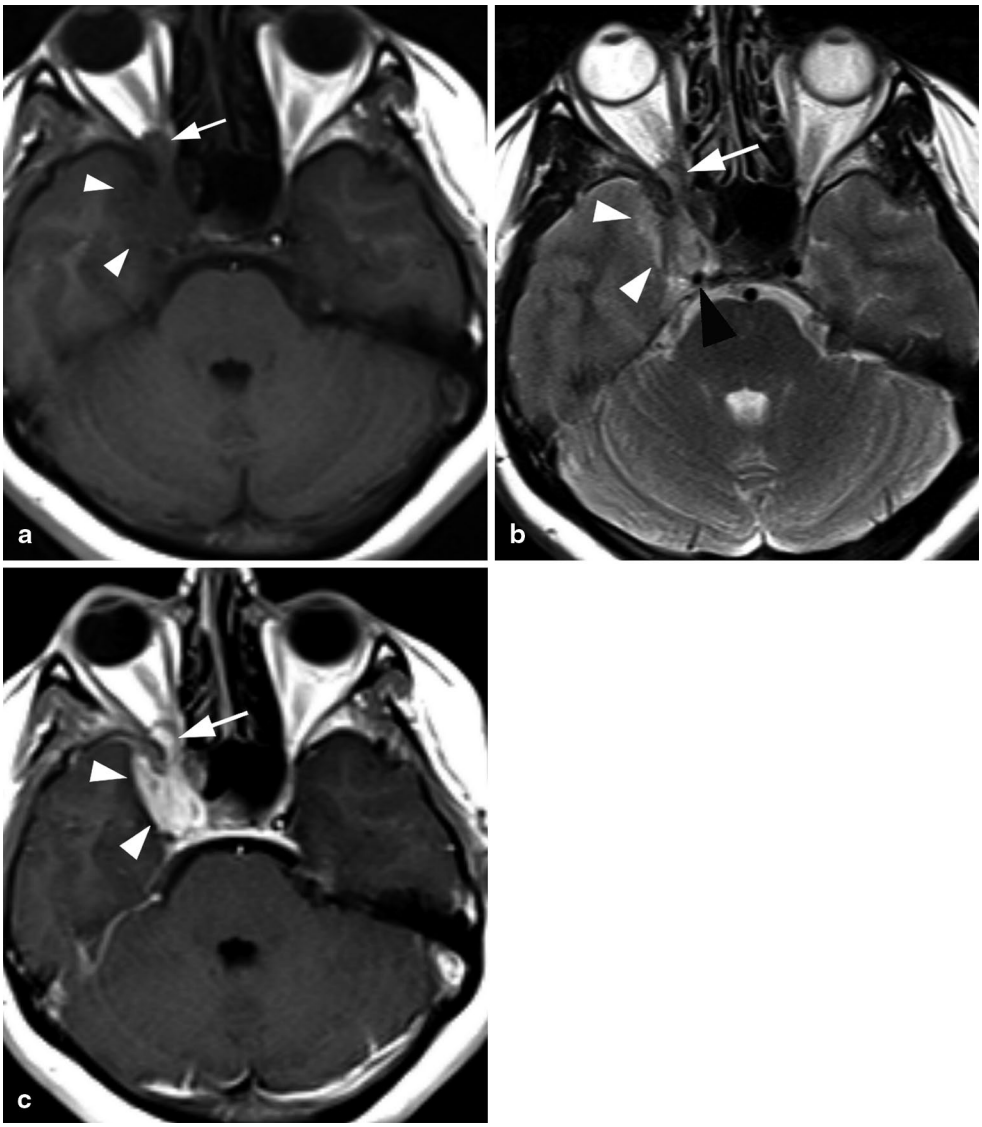

Fig. 4 Meningioma originating from sphenoid wing. Axial T1W (**a**) and T2W (**b**) MR images show a meningioma originating from the right greater wing of the sphenoid bone and extending into the right CS (*arrowheads* in **a**, **b**) and the orbital apex via the superior orbital fissure (*arrow* in **a**, **b**). Note that the right ICA is compressed by the meningioma (*black arrowhead* in **b**). **c** The axial postcontrast T1W MR image shows the right exophthalmos and the asymmetric enlargement and intense enhancement of the right CS (*arrowheads*) and the orbital apex (*arrow*)

Chordoma

Chordomas are midline lesions that usually arise in the clivus and are derived from remnants of the notochord [30]. They are considered to be locally invasive neoplasms and frequently show extension into the CS [30]. On T1W images, chordomas display low to intermediate signals, with occasional areas of high signal intensity attributable to mucinous material and hemorrhage within the tumor. On T2W images, chordomas display very high signal intensity. The intratumoral hypointense areas commonly seen on T2W images are a result of intralesional hemosiderin and calcification. In most cases, a mildly heterogeneous contrast enhancement pattern is observed. Computed tomography (CT) provides very precise imaging of the tumor-induced destruction of bones (Fig. 9).

Chondrosarcoma

Intracranial chondrosarcomas are rare tumors that arise from mesenchymal cells or fetal cartilage within the skull base. While intracranial chordomas are located along the midline, chondrosarcomas originate laterally along the petro-occipital, spheno-occipital, sphenopetrosal, or sphenoethmoidal fissure and grow into the midline [31]. The most frequently detected "petroclival" type of chondrosarcoma has a characteristic connection to the CS [31, 32]. Chondrosarcomas usually present as hypointense lesions on T1W images and as hyperintense lesions on T2W images. They show mild to marked heterogeneous enhancement on both sequences. While intratumoral hemorrhage and proteinaceous mucus result in a high signal focus on T1W images, chondroid matrix mineralization gives rise to a low signal focus on T2W images. Ring-and-arc calcification patterns on CT scans and ring-and-arc enhancement

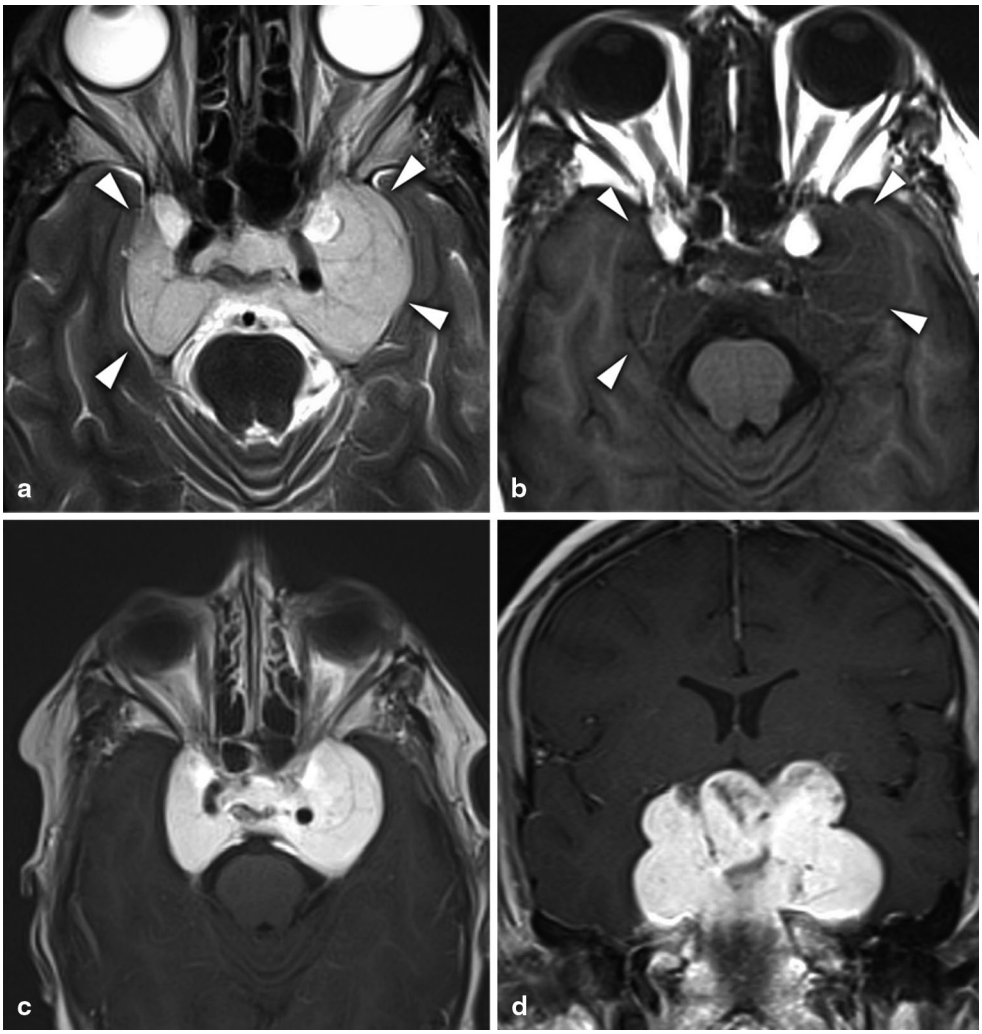

Fig. 5 A cavernous hemangioma in a 40-year-old woman. **a** The axial T2W MR image shows a well-defined, homogenous, markedly hyperintense mass that originates from the CS and expands to the sellar and parasellar regions (*arrowheads*). **b** An axial T1W MR image shows that the mass is isointense and surrounds the bilateral CSs of the ICA (*arrowheads*). **c**, **d** Contrast-enhanced T1W MR images show that the mass enhancement is homogenous

patterns on MR images strongly indicate a diagnosis of chondrosarcoma because of the characteristic chondroid mineralization.

Fibrous Dysplasia

Approximately 25 % of fibrous dysplasia lesions arise from the base of the skull, and those that extend to the CS usually involve the sphenoid body and clivus [33]. On a CT scan, the affected bone displays expansion with characteristic "ground-glass" opacity [34]. Cranial base fibrous dysplasia appear hypointense on T1W MR images in almost all cases, while their signal intensity on T2W images ranges from high to low. Because of their prominent vascularization, these tumors are often enhanced on contrast administration.

Juvenile Angiofibroma

Juvenile angiofibroma is a histologically benign but locally invasive vascular tumor that invades many critical intracranial structures. However, the tumor may extend into the CS by expanding along a canal or through areas of bone destruction [35]. MR imaging is an excellent technique for assessing tumor extension. Prominent and homogeneous enhancement and flow voids within the lesion on contrast administration are characteristics of juvenile angiofibroma. On both T1 and T2 sequences, the signal intensity of the tumor ranges from low to intermediate.

Lymphoma

Lymphoma may involve the CS as a result of either invasion or metastasis originating in the head and neck region or metastasis of systemic origin [36]. The occurrence of lymphoma as a primary CS tumor is only infrequently reported in the literature [36–38]. The following MR imaging findings indicate an infiltrative lesion: involvement of the CS without arterial narrowing, obliteration or replacement of the clivus by the mass, and iso- or hypointensity on both T1W and T2W images with bright enhancement (Fig. 10). Enhancement along the dural surface may also

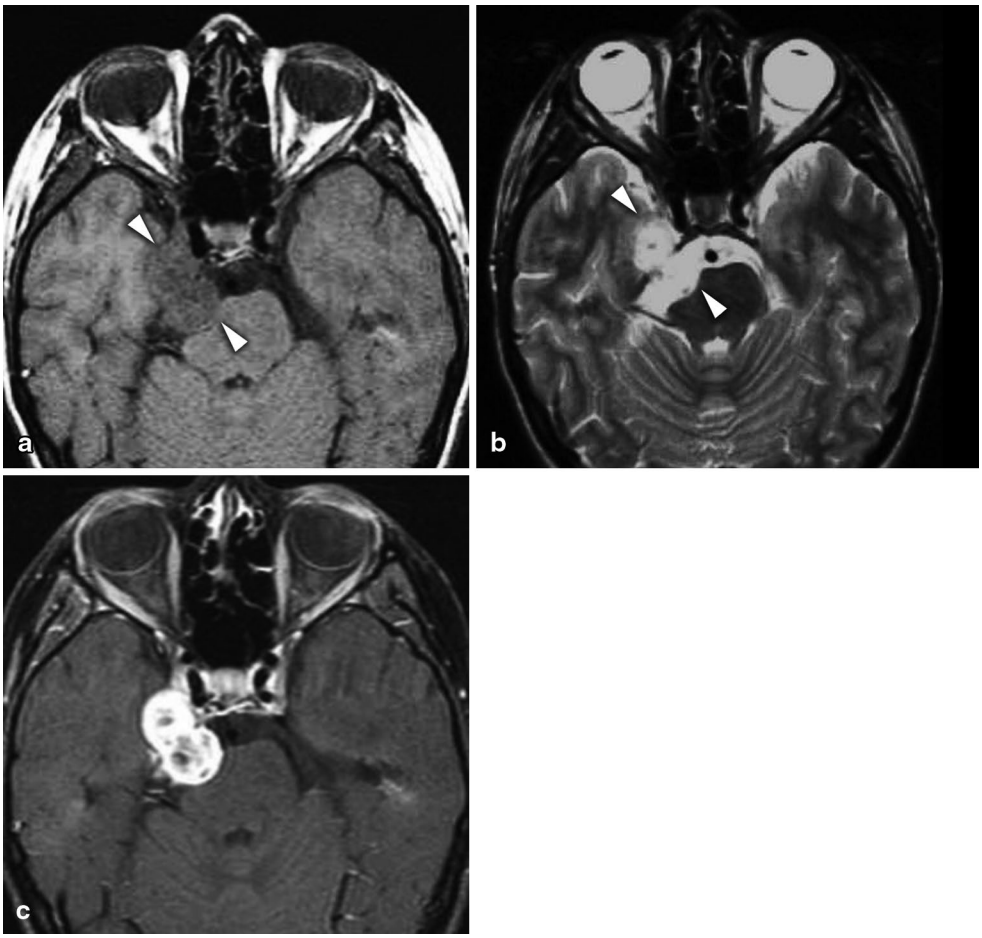

Fig. 6 Schwannoma. **a** The axial T1W MR image shows a hypointense schwannoma filling the right inferior portion of the CS and Meckel's cave and extending along the cisternal part of the fifth nerve, causing a dumbbell-shaped appearance (*arrowheads*). The axial T2W MR image (**b**) shows that the schwannoma is hyperintense (*arrowheads*), and the axial contrast-enhanced T1W MR image (**c**) shows that the schwannoma is intensely enhanced

be noted on postcontrast images, similar to the "dural tail sign" previously described for meningiomas [39]. Dural tails are usually observed in cases of primary lymphomas. Therefore, it is sometimes difficult to distinguish primary CS lymphomas from CSMs on the basis of radiologic evaluation alone.

Congenital Cystic Tumors

Epidermoid Cyst

Intracranial epidermoid cysts, which are relatively rare compared with all of the intracranial tumors, mostly originate from the cerebellopontine angle. The CS is an uncommon location for epidermoid cysts. Gharabaghi et al. [40] have suggested that there are three types of epidermoid cysts within the CS in their classification system. The first type has an extracavernous (petrous apex or parasellar) origin and invades the CS. The second group consists of intradural cysts that arise from the lateral CS wall. The third type of cysts is primary intracavernous epidermoid tumors. Epidermoid cysts display specific imaging characteristics, and they appear distinctly hyperintense on fluid-attenuated inversion recovery sequence and demonstrate restricted diffusion with higher signal intensity than that of cerebrospinal fluid (CSF) on diffusion-weighted sequence. Most of them are hypointense on T1W images and hyperintense on T2W images (Fig. 11).

Dermoid Cyst

Cavernous dermoid cysts are extremely unusual tumors that are predominantly located intradurally between the inner and outer layers of the lateral wall [41]. Typically, the intracavernous ICA is displaced by a circular or oval mass, without marked narrowing [41]. On MR imaging, the heterogeneous texture of dermoid cysts, which results from their hair and fat contents and their sebaceous contents, result in their characteristic hyperintense T1 signals.

Rathke Cleft Cyst

Rathke cleft cysts, which are embryologic remnants of Rathke's pouch, rarely extend into the CS without invading it. Although patients with these intrasellar cysts are gener-

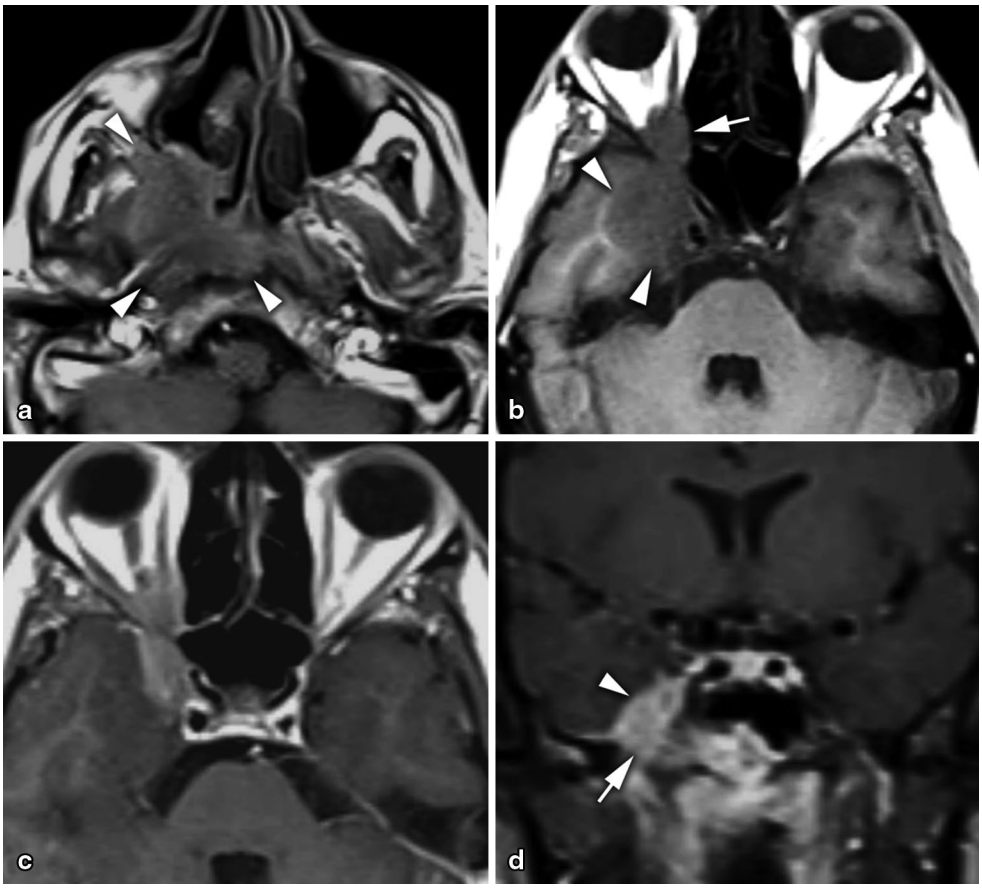

Fig. 7 Nasopharynx carcinoma. **a** Axial T1W MR image show a hypointense lesion arising from the right portion of the nasopharynx and extending to the right pterygoid fossa (*arrowheads*). **b** The lesion extends to the right CS (*arrowheads*) and the orbital apex via the superior orbital fissure (*arrow*) on axial T1W MR image. **c** The mass enhances heterogeneously on axial contrast-enhanced T1W MR image. **d** Note the enhancement in the foramen ovale (*arrow*) that is compatible with perineural spread of nasopharynx carcinoma to the Meckel's cave and CS (*arrowhead*) on a coronal contrast-enhanced T1W MR image

ally asymptomatic, they present with CS syndrome when the cysts expand into the CS [42]. The Rathke cleft cysts show various T1 and T2 signal intensities that are dependent on the composition of the cystic fluid. In the presence of an intracystic nodule that is clearly visible as hypointense on T2W imaging and hyper- or isointense on T1W imaging, MR imaging permits the diagnosis of a Rathke cleft cyst.

Vascular Lesions

Aneurysms

Internal carotid aneurysms that occur in the cavernous segment most commonly originate from the anterior genu, which is followed in prevalence by origination from the horizontal part and then the posterior genu [43]. Cavernous ICA aneurysms tend to be asymptomatic. However, these aneurysms can be large, and they often produce cranial neuropathy symptoms that are related to a mass effect [43]. Despite a tendency for a benign clinical course, aneurysms can lead to life-threatening complications, including subarachnoid hemorrhages, carotid cavernous fistulas (CCFs), serious epistaxis, cerebral infarcts, and distal ischemia [43, 44]. Cavernous ICA aneurysms have variable presentations on CT and MR imaging examinations due to their variable sizes, morphologies, stage of thrombosis, calcification, and flow velocity (Fig. 12). On unenhanced CT scans, the aneurysm appears as a mildly hyperdense mass, and it may exhibit peripheral calcification along the aneurysmal wall or linear calcifications within the chronic thrombus. High aneurysmal velocity flow can demonstrate characteristic flow void within the aneurysm on spin-echo MR imaging sequences [44]. Conversely, slow-flow aneurysms, which may not show flow void, may appear as a solid mass that presents homogeneous central enhancement [44]. In cases that do not show flow void, a pulsation artifact along the phase-encoding axis is an indicator of the vascular nature of the lesion. Furthermore, if there is a complex flow pattern within the aneurysm, prominent heterogeneous signal intensities can be detected on T1W and T2W images [44].

Carotid Cavernous Fistula

CCFs are abnormal vascular connections that allow blood to flow from the high-velocity carotid artery into the low-

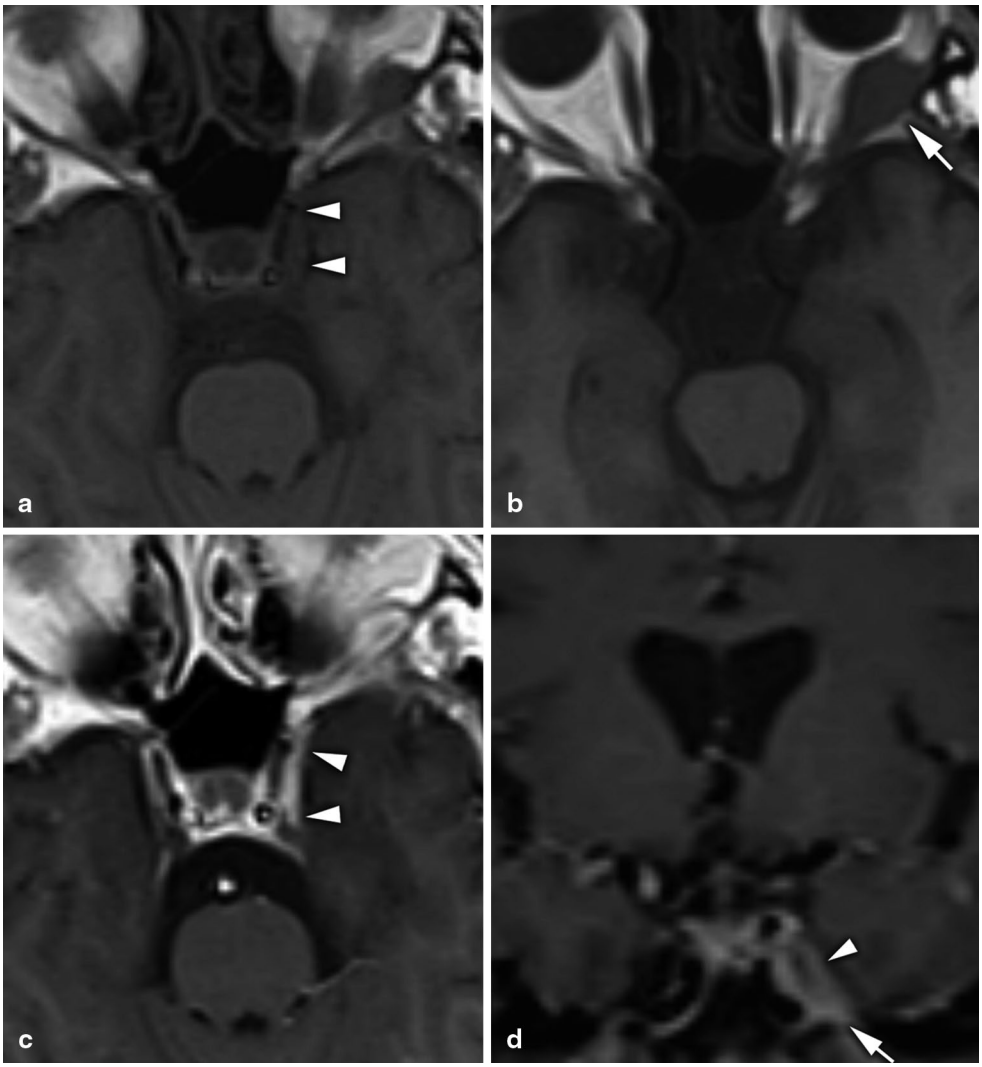

Fig. 8 CS and orbital metastasis from breast carcinoma. **a**, **b** Axial T1W MR images show enlargement and a loss of normal hyperintense fat signal of the left CS (*arrowheads* in **a**) and a mass lesion on the lateral aspect of the left orbit arising from the lateral rectus muscle (*arrow* in **b**). **c**, **d** Contrast-enhanced T1W MR images show intense asymmetric enhancement of the left CS (*arrowheads* in **c**, **d**) and left mandibular nerve passing through the foramen ovale (*arrow* in **d**), which suggests invasion by the mass

flow CS. CCFs have been categorized based on their arterial anatomy, etiology, and/or hemodynamic features. Anatomical classifications describe direct fistulas as those that originate from the carotid artery, while indirect fistulas are those that arise from the meningeal branches of the carotid artery [45]. Etiological classifications categorize fistulas into spontaneous or traumatic fistulas [46]. Hemodynamic classifications distinguish high-flow from low-flow fistulas. Barrow et al. [47] have classified these into four types based on their detailed anatomical classification. Type A fistulas are direct shunts between the ICA and the CS, and they generally exhibit high flow (Fig. 13). Indirect fistulas are also called dural fistulas, and they are fed by the dural branches of the ICA (type B), the dural branches of the external carotid artery (type C), or both (type D). In addition, they are typically associated with low-flow ratios. Traumatic fistulas are usually type-A fistulas, and these are the most common type of CCFs [46]. They are typically found because of a basilar skull fracture. Spontaneous CCFs are direct fistulas that often arise from ruptured cavernous ICA aneurysms. The other predisposing conditions for direct type-A fistulas include fibromuscular dysplasia, hypertension, collagen vascular diseases, and atherosclerotic disease. While cerebral angiography is the gold standard imaging technique, noninvasive imaging with CT, MR imaging, CT/MR angiography, or time-resolved MR angiography is performed in the initial diagnostic workup of a possible CCF. The radiographic appearance of CCFs is related to the type of venous drainage, either anterior into the ophthalmic veins or posterior into the petrosal sinuses. CT and MR imaging findings that are found with variable frequencies include enlargement of the CS, dilation of the superior ophthalmic vein, occlusion of the sphenoparietal vein and petrosal sinuses, diffuse thickening of the extraocular muscle, edema in the retro-orbital fat, and proptosis [48]. Spin-echo and gradient-echo MR images provide additional information by detecting flow voids in the CS. On spin-echo MR images, in the presence of a CCF, it might be difficult to discriminate variable normal venous signals due to the different venous flow ratios in the CS from abnormal signal voids. In that case, the

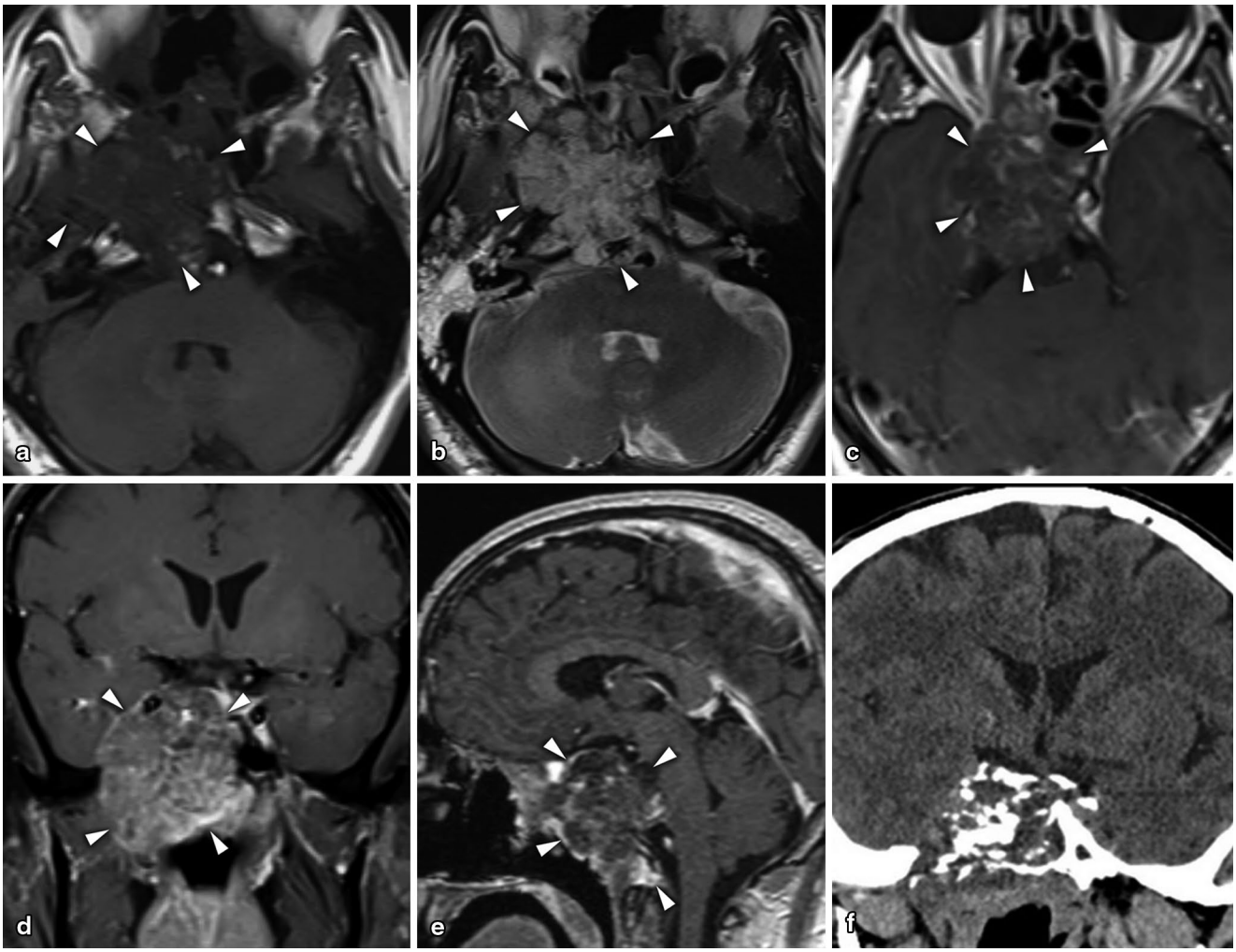

Fig. 9 Chordoma. **a** An axial T1W MR image shows a hypointense mass originating from the clivus (*arrowheads*). **b** The T2W MR image shows the mass is markedly hyperintense, extending into the right CS and prepontine cistern (*arrowheads*). **c**, **d**, **e** Postcontrast T1W MR images shows mild heterogeneous enhancement of the mass involving the right CS, Meckel's cave, and infratemporal fossa (*arrowheads* in **c**, **d**, **e**). **f** A coronal CT image shows clival destruction and mass calcification

visualization of flow-related hyperintense signals within the CS on the source images of unenhanced three-dimensional time-of-flight MR angiography can be extremely helpful in the diagnosis of CCFs [49].

Thrombosis

CS thrombosis (CST) is a rare but potentially lethal disease that has been classified into aseptic and septic types based on its etiology. Aseptic thrombosis can result from trauma, vascular conditions (such as aneurysm or CCF), surgery, tumor growth, hematological disease, or hypercoagulable states [50]. Septic thrombosis is among the most frequent causes of CST, and they can be defined as CS thrombophlebitis. Sphenoethmoidal sinusitis, which is followed by facial cutaneous infection, is the most frequent cause of septic CST, with *Staphylococcus aureus* as the leading responsible microorganism [51]. Although all infections of the head and neck, including the sinuses, face, oral cavity, orbits, and skull base, can spread to the CS, septic CST rarely arises from distant infection. CT and MR imaging examinations provide clues about CST from direct signs, including an enlarged CS with lateral margin convexity or flattening in contrast to normal concavity and multiple irregular filling defects within the heterogeneous enhancing sinus [52–54]. Additionally, indirect signs that are associated with concomitant venous occlusion can be seen, and these include expansion of the superior ophthalmic vein, orbital edema, exophthalmos, and filling defects that indicate thrombus within the superior ophthalmic vein and adjacent tributaries [52–54]. Acute CST appears as abnormal soft tissue with variable signals, and a subacute thrombus may be visualized as T1 hyperintensity in the affected CS. Postcontrast MR imaging can also identify meningeal enhancement along the lateral wall of the sinus.

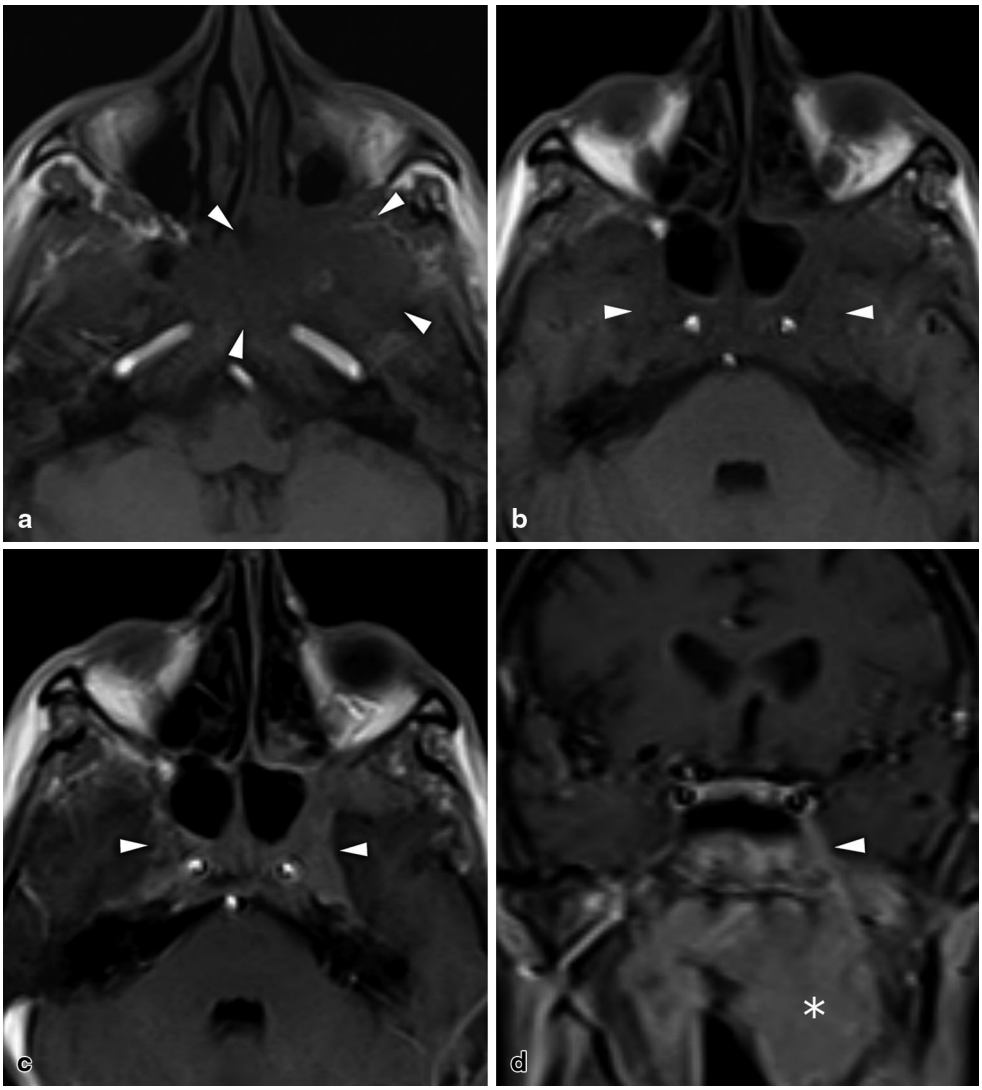

Fig. 10 Non-Hodgkin lymphoma originating from the nasopharynx. **a** An axial T1W MR image shows a large hypointense mass originating from the nasopharynx (*arrowheads*). Axial T1W (**b**) MR image shows involvement of bilateral CSs (*arrowheads* in **b**) with heterogeneous, intense enhancement (*arrowheads*) on the postcontrast T1W MR image (**c**). **d** A coronal contrast-enhanced T1W MR image shows extension of the left Meckel's cave and CS (*asterisk*) through the foramen ovale (*arrowhead*) via perineural spread

Infectious, Inflammatory, and Granulomatous Lesions

Tolosa–Hunt Syndrome

Tolosa–Hunt syndrome is defined as a recurrent painful ophthalmoplegia that is caused by chronic granulomatous inflammation of the CS [55, 56]. This condition usually presents with acute-onset unilateral orbital pain and oculomotor paralysis that typically and promptly responds to corticosteroid therapy. Thin-section contrast-enhanced MR imaging with fat suppression is considered to be the best imaging method to demonstrate enlargement of the CS from the brightly enhanced abnormal soft tissue, which is isointense on T1W and iso- to hypointense on T2W images [57, 58]. Furthermore, involvement of the orbital apex, the superior orbital fissure, and extraocular muscles (Fig. 14); narrowing of the intracavernous ICA; and perineural and dural enhancement may be seen [57, 58].

Tolosa–Hunt syndrome is hypothesized to be part of a spectrum of disorders that occur in different regions but that have similar histologic and imaging findings [59–63]. Inflammatory myofibroblastic tumors and idiopathic hypertrophic pachymeningitis are the other disorders in this spectrum. The radiologic appearances of these three diseases may overlap most often when they involve the CS.

An inflammatory myofibroblastic tumor is characterized by inflammatory cells that have varying degrees of fibrous reactions. This process can appear in any site of the human body, including the orbits and meninges. When an inflammatory myofibroblastic tumor occurs in the orbit, it may progress to infiltrate the CS, resulting in MR imaging findings that are similar to Tolosa–Hunt syndrome [59]. However, when the tumor occurs in the meninges, it can lead to localized or diffuse intracranial dural thickening, which is a typical imaging finding of idiopathic hypertrophic pachymeningitis [60].

Idiopathic hypertrophic pachymeningitis is a rare chronic inflammatory fibrosis of the dura mater that results in dif-

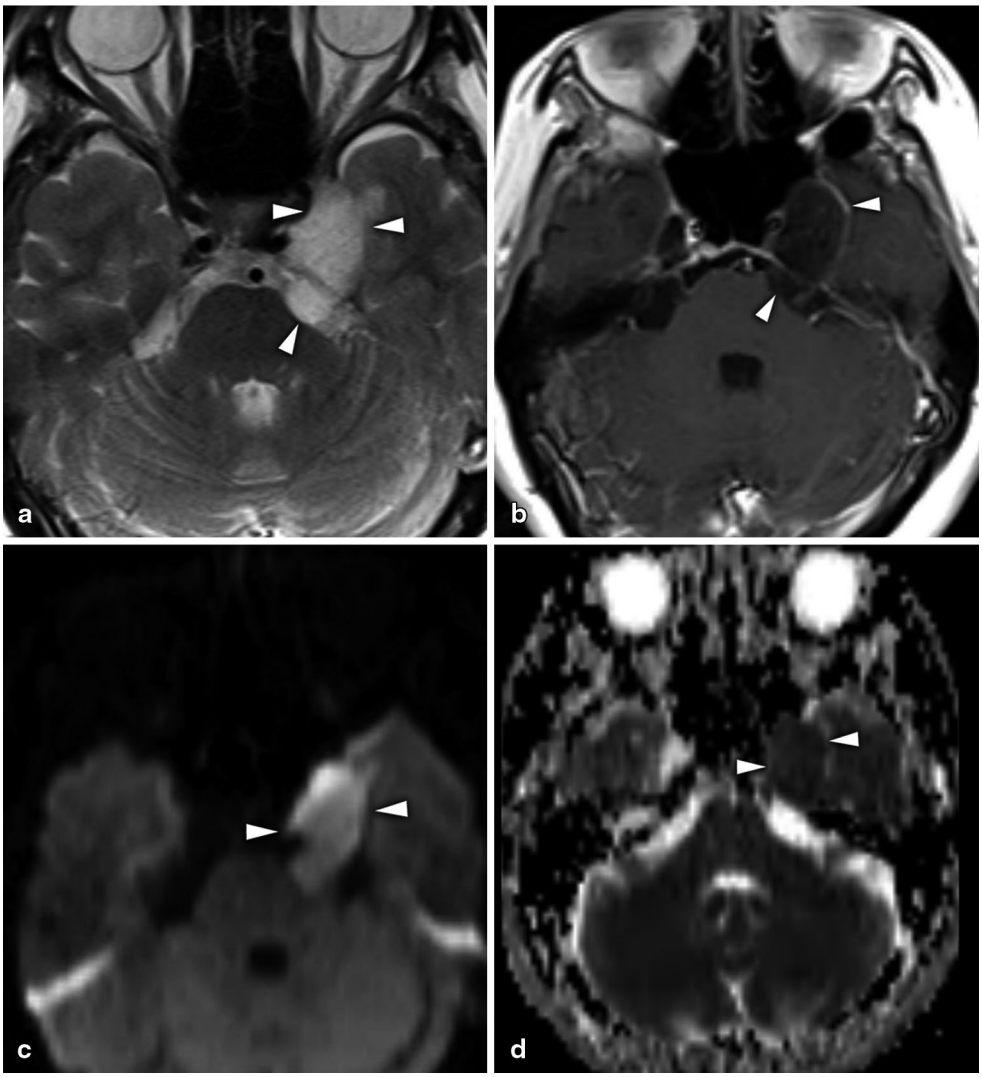

Fig. 11 Epidermoid cyst. An axial T2W MR image (**a**) shows a heterogeneous hyperintense space-occupying cystic lesion arising from the lateral wall of the left CS (*arrowheads*), and a contrast-enhanced T1W MR image (**b**) shows no contrast enhancement (*arrowheads*). Diffusion-weighted MR image (**c**) and corresponding apparent diffusion coefficient map (**d**) show significant diffusion restriction within the lesion indicative of epidermoid cysts (*arrowheads* in **c**, **d**)

fuse thickness and that may extend into the CS. Isolated cases of Tolosa–Hunt syndrome have been reported to have simultaneous pachymeningitis [61]. Conversely, cases with idiopathic hypertrophic pachymeningitis with concurrent orbital mass have been reported [62].

Furthermore, a unique case, which has been reported in the literature, showed the typical imaging findings of each of these three fibroinflammatory disease simultaneously: CS prominence (typically seen with Tolosa–Hunt syndrome), orbital mass (characteristic of an inflammatory myofibroblastic tumor), and dural thickening (indicative of idiopathic hypertrophic pachymeningitis) [63]. This case seems to support the hypothesis that these disorders are part of a spectrum.

IgG4-Related Disease

IgG4-related disease is a recently recognized fibroinflammatory systemic condition characterized by elevated serum IgG4 levels and mass lesions with characteristic pathologic features, including storiform fibrosis with IgG4-positive lymphoplasmacytic infiltration [64]. IgG4-related disease typically affects the pancreas, salivary glands, and lacrimal glands. However, rare cases of IgG4-related disease involving the central nervous system (CNS), including the CS and meninges, have been reported. [64]. The orbital IgG4-related disease symptoms often present with subacute- or chronic-onset lid swelling and proptosis with mild signs or no signs of orbital pain [65]. MR imaging demonstrates mass lesions in the CS usually together with diffuse concentric thickening of the V_1 and V_2 nerves. Furthermore, multiple infraorbital nodules and concentric thickening of the infraorbital nerve can be observed. All the lesions are hypointense on T2W images, and they demonstrate marked enhancement on postcontrast series [64].

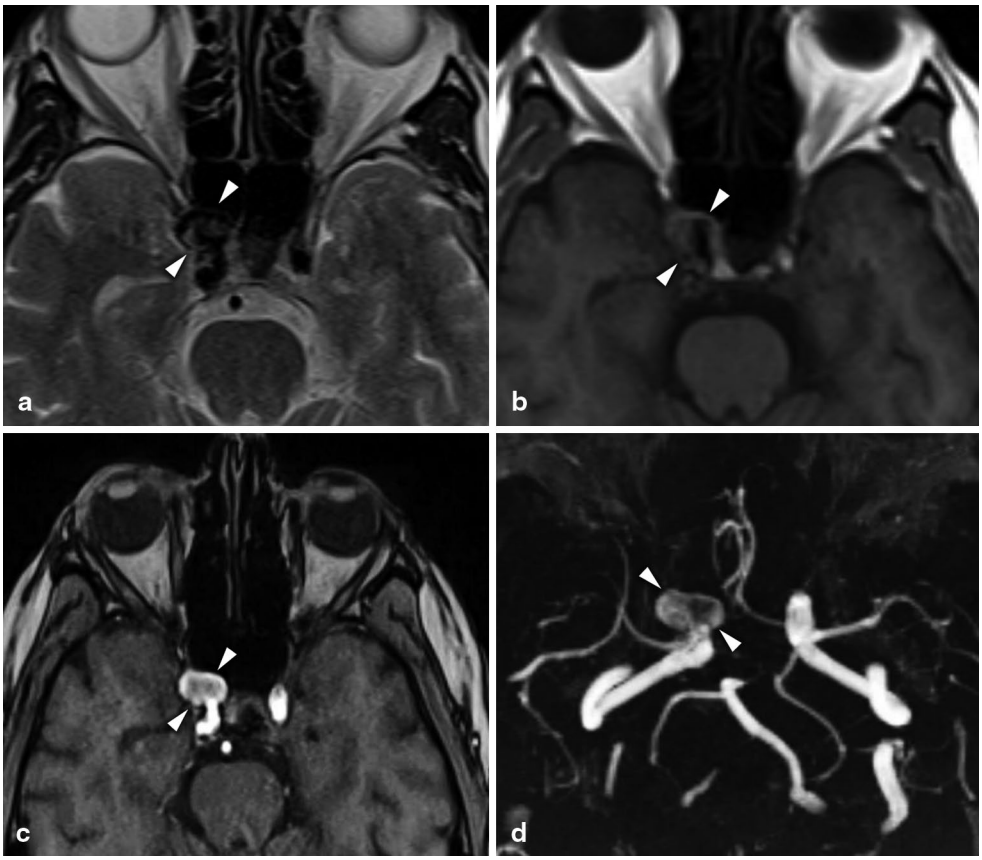

Fig. 12 Cavernous ICA aneurysm. Axial T2W (**a**) and contrast-enhanced T1W (**b**) MR images show an expansile lesion in the right CS (*arrowheads* in **a**, **b**). Axial maximum intensity projection image (**c**) and time-of-flight magnetic resonance angiogram (**d**) show the aneurysm originating from the right cavernous segment of the ICA (*arrowheads* in **c**, **d**)

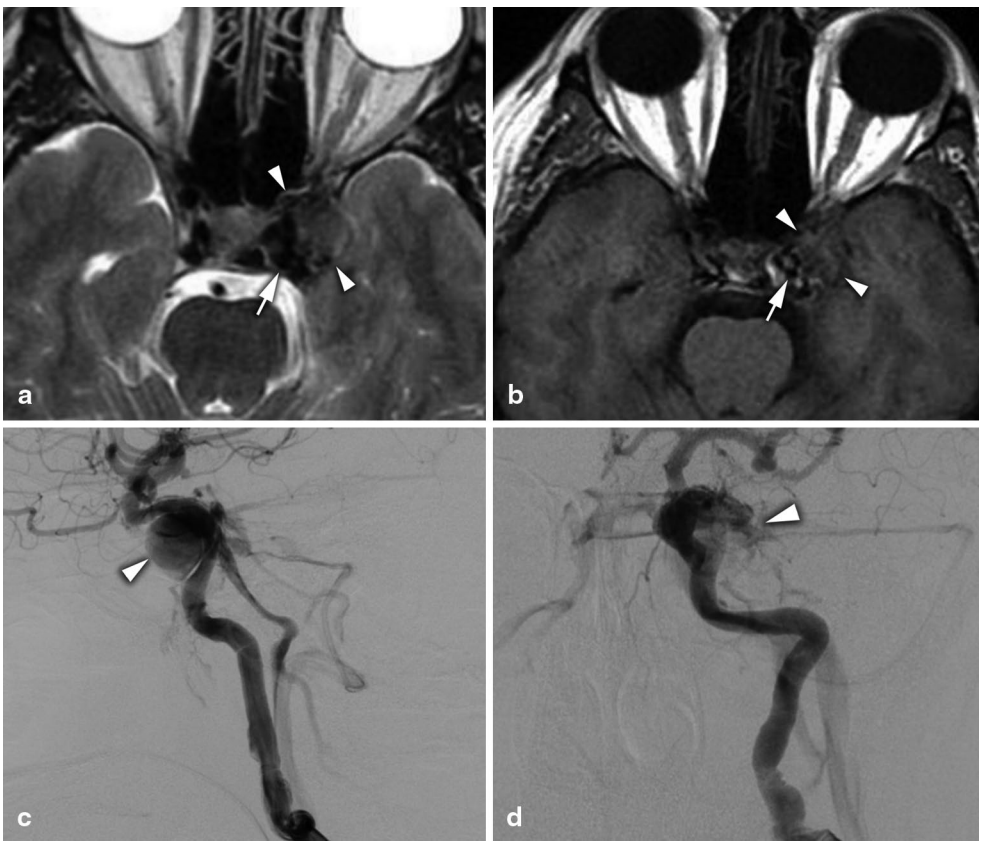

Fig. 13 Direct carotid cavernous fistula (CCF) with fibromuscular dysplasia. Axial T2W (**a**) and axial T1W (**b**) MR images show asymmetric enlargement of the left CS (*arrowheads* in **a**, **b**) with abnormal signal voids (*arrows* in **a**, **b**), indicating a CCF due to the traumatic rupture of the aneurysm of the cavernous ICA. **c**, **d** Digital subtraction angiography images show the aneurysm on the CS of the left ICA (*arrowhead* in **c**) and a direct type of CCF (*arrowhead* in **d**)

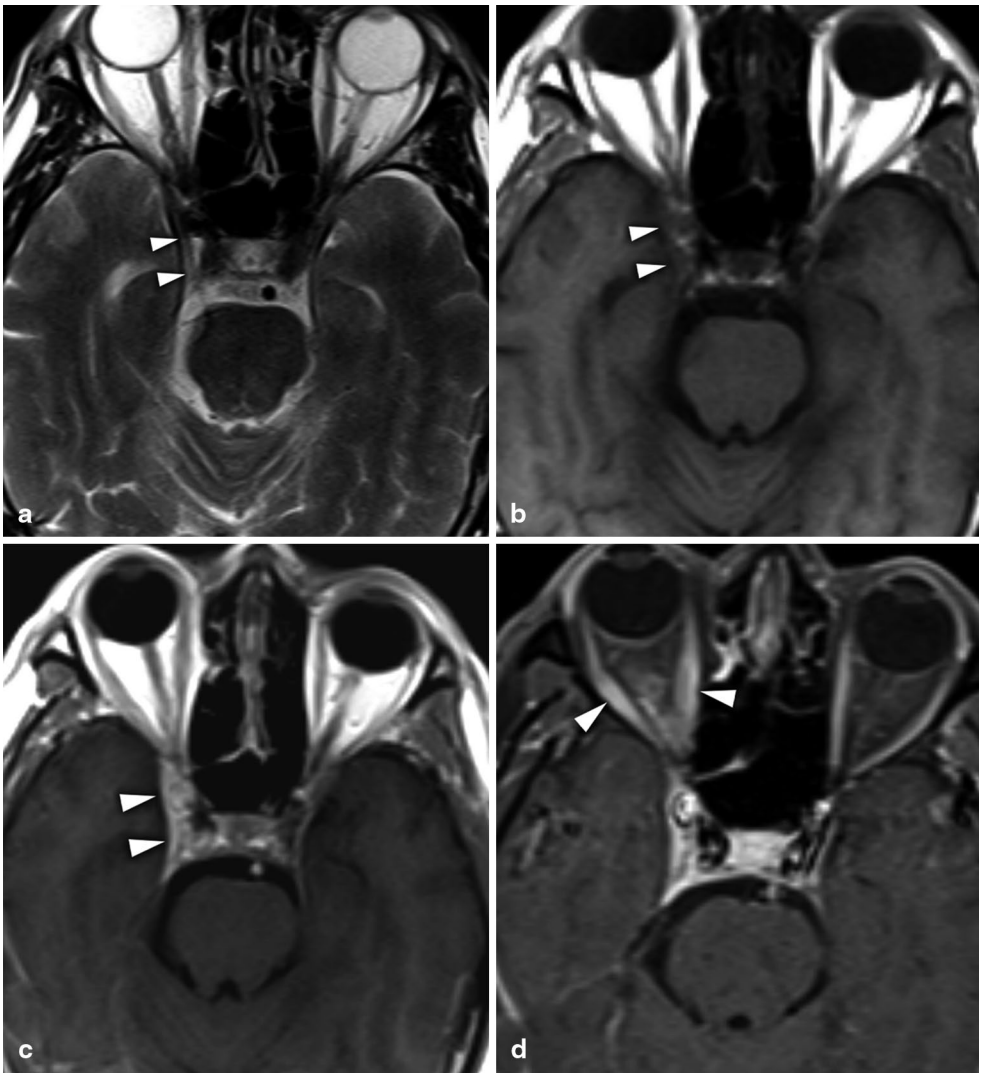

Fig. 14 Tolosa–Hunt syndrome with ptosis. An axial T2W MR image (**a**) shows hyperintense inflammatory soft tissue within the right CS (*arrowheads*) that is hypointense (*arrowheads*) on a T1W image (**b**). Axial postcontrast T1W (**c**) and fat-saturated T1W (**d**) MR images show asymmetric enlargement and enhancement in the right CS (*arrowheads* in **c**). Note the soft tissue extending into the right orbital apex, extraocular muscles, and retro-orbital fat via the superior orbital fissure (*arrowheads* in **d**)

Wegener's Granulomatosis

Wegener's granulomatosis is a systemic necrotizing vasculitis that primarily affects the lungs and kidneys. CS involvement, which is unusual in Wegener's granulomatosis, may occur by three coexisting pathologic mechanisms: vasculitis, subsequent invasion from the paranasal sinus, orbital or nasal granulomatous sites, or primary intracavernous granulomatous inflammation [66]. On T2W MR images, the CS demonstrates low signal intensity due to the fibrous nature of the inflammatory process. After contrast administration, homogeneous enhancement is seen.

Sarcoidosis

Sarcoidosis, which is an idiopathic inflammatory disorder with noncaseating granuloma formation, can affect any organ in the body and occasionally the CS. Contrast-enhanced MR images demonstrate an enhanced mass within the CS with meningeal and retro-orbital enhancement [67]. The signal intensity is usually isointense on T1W images and low on T2W images, which may result in the misdiagnosis of meningioma or inflammatory myofibroblastic tumor.

Tuberculosis

CNS tuberculosis can occur in various forms, such as tuberculous meningitis, tuberculous encephalitis, intracranial tuberculomas, and abscesses. CS involvement is extremely rare and may occur primarily or secondarily to pulmonary or cervical lymph node tuberculosis [68]. Most CS tuberculomas appear isointense on T1W MR images and hypointense on T2W sequences with dural thickening. On a postcontrast series, pachymeningeal and lesional enhancement can be seen. These MR imaging findings of tuberculosis, especially isolated ones without systemic tuberculosis, can be misdiagnosed as a meningioma [69].

Conclusion

The CS contains crucial anatomical structures that can be invaded by neoplastic, infectious, inflammatory, and vascular processes. A precise knowledge of the complex anatomy of the CS, together with pathological processes and their imaging characteristics, will enable accurate evaluations of the conditions that affect the CS (Table. 1).

Table 1 Key imaging findings of common pathologic conditions of the cavernous sinus

Diagnosis	Key imaging findings
Pituitary adenoma	Sellar origin Less enhancement compared with the normal pituitary gland Encasement of the intracavernous ICA
Meningioma	Hyperostosis or dural involvement Constricting of the adjacent ICA
Hemangioma	Markedly high T2 signal intensity Peripheral to central "filling in" enhancement
Schwannoma	Dumbbell-shaped appearance Origin of the trigeminal nerve, the oculomotor nerve, and, rarely, the abducens nerve
Nasopharyngeal carcinoma	Nasopharyngeal origin Perineural spread Extension directly via the skull base erosion
Metastases	Cavernous sinus origin Hematogenous or perineural spread Primary malignant tumors
Chordoma	Clival origin Bone destruction and intralesional calcification
Chondrosarcoma	Petroclival origin Ring-and-arc calcification patterns Ring-and-arc enhancement patterns
Juvenile angiofibroma	Flow voids within the lesion
Lymphoma	Iso- or hypointensity on both T1- and T2-weighted images with bright enhancement Dural tail sign
Epidermoid cyst	Restricted diffusion Higher signal intensity than that of cerebrospinal fluid on diffusion-weighted sequence
Dermoid cyst	Interdural origin Hyperintense T1 signal
Aneurysms	Cavernous ICA origin Flow void on spin-echo MR imaging Pulsation artifact along the phase-encoding axis
Carotid cavernous fistula	Dilation of the superior ophthalmic vein Occlusion of the sphenoparietal vein and petrosal sinuses Abnormal flow voids in the CS on spin-echo MR images Flow-related hyperintense signals within the CS on the time-of-flight MR angiography
Thrombosis	Lateral margin convexity or flattening of the CS Multiple irregular filling defects within the CS
Tolosa–Hunt syndrome	Involvement of the orbital apex, the superior orbital fissure, and extraocular muscles

ICA internal carotid artery, *MR* magnetic resonance, *CS* cavernous sinus

References

1. Campero A, Campero AA, Martins C, Yasuda A, Rhoton AL, Jr. Surgical anatomy of the dural walls of the cavernous sinus. J Clin Neurosci. 2010;17:746–50.
2. Jinkins JR. Atlas of neuroradiologic embryology, anatomy, and variants. 1st ed. Philadelphia: Lippincott Williams & Wilkins; 2000.
3. Liang L, Gao F, Xu Q, Zhang M. Configuration of fibrous and adipose tissues in the cavernous sinus. PLoS One. 2014;9:e89182.
4. Yagi A, Sato N, Taketomi A, Nakajima T, Morita H, Koyama Y, Aoki J, Endo K. Normal cranial nerves in the cavernous sinuses: contrast-enhanced three-dimensional constructive interference in the steady state MR imaging. AJNR Am J Neuroradiol. 2005;26:946–50.
5. Ahmadi J, North CM, Segall HD, Zee CS, Weiss MH. Cavernous sinus invasion by pituitary adenomas. AJR Am J Roentgenol. 1986;146:257–62.
6. Thapar K, Kovacs K, Scheithauer BW, Stefaneanu L, Horvath E, Pernicone PJ, Murray D, Laws ER, Jr. Proliferative activity and invasiveness among pituitary adenomas and carcinomas: an analysis using the MIB-1 antibody. Neurosurgery. 1996;38:99–106.
7. Heck A, Ringstad G, Fougner SL, Casar-Borota O, Nome T, Ramm-Pettersen J, Bollerslev J. Intensity of pituitary adenoma on T2-weighted magnetic resonance imaging predicts the response to octreotide treatment in newly diagnosed acromegaly. Clin Endocrinol (Oxf). 2012;77:72–8.
8. Knosp E, Steiner E, Kitz K, Matula C. Pituitary adenomas with invasion of the cavernous sinus space: a magnetic resonance imaging classification compared with surgical findings. Neurosurgery. 1993;33:610–8.
9. Cottier JP, Destrieux C, Brunereau L, Bertrand P, Moreau L, Jan M, Herbreteau D. Cavernous sinus invasion by pituitary adenoma: MR imaging. Radiology. 2000;215:463–9.
10. Vieira JO, Jr., Cukiert A, Liberman B. Evaluation of magnetic resonance imaging criteria for cavernous sinus invasion in patients with pituitary adenomas: logistic regression analysis and correlation with surgical findings. Surg Neurol. 2006;65:130–5.
11. Cao L, Chen H, Hong J, Ma M, Zhong Q, Wang S. Magnetic resonance imaging appearance of the medial wall of the cavernous sinus for the assessment of cavernous sinus invasion by pituitary adenomas. J Neuroradiol. 2013;40:245–51.
12. Felippu A, Mora R, Guastini L, Peretti G. Transnasal approach to the orbital apex and cavernous sinus. Ann Otol Rhinol Laryngol. 2013;122:254–62.
13. Molitch ME, Cowen L, Stadiem R, Uihlein A, Naidich M, Russell E. Tumors invading the cavernous sinus that cause internal carotid artery compression are rarely pituitary adenomas. Pituitary. 2012;15:598–600.
14. Heth JA, Al-Mefty O. Cavernous sinus meningiomas. Neurosurg Focus. 2003;14:e3.
15. Ruscalleda J. Imaging of parasellar lesions. Eur Radiol. 2005;15:549–59.
16. Sepehrnia A, Tatagiba M, Brandis A, Samii M, Prawitz RH. Cavernous angioma of the cavernous sinus: case report. Neurosurgery. 1990;27:151–5.
17. Rosenblum B, Rothman AS, Lanzieri C, Song S. A cavernous sinus cavernous hemangioma. Case report. J Neurosurg. 1986;65:716–8.
18. Hasiloglu ZI, Asik M, Kizilkilic O, Albayram S, Islak C. Cavernous hemangioma of the cavernous sinus misdiagnosed as a meningioma: a case report and MR imaging findings. Clin Imaging. 2013;37:744–6.
19. Zhang L, Yang Y, Xu S, Wang J, Liu Y, Zhu S. Trigeminal schwannomas: a report of 42 cases and review of the relevant surgical approaches. Clin Neurol Neurosurg. 2009;111:261–9.

20. Hayashi M, Chernov M, Tamura N, Yomo S, Ochiai T, Nagai M, Tamura M, Izawa M, Muragaki Y, Iseki H, Okada Y, Takakura K. Gamma Knife surgery for abducent nerve schwannoma. Report of 4 cases. J Neurosurg. 2010;113:136–43.
21. Shibao S, Hayashi S, Yoshida K. Dumbbell-shaped abducens Schwannoma: case report. Neurol Med Chir (Tokyo). 2014;54:331–6.
22. Gholkar A, Stack JP, Isherwood I. Plexiform trigeminal neurofibroma. Clin Radiol. 1988;39:313–5.
23. Visrutaratna P, Oranratanachai K, Singhaveisakul J. Clinics in diagnostic imaging. Plexiform neurofibromatosis. Singapore Med J. 2004;45:188–92.
24. Lee JH, Lee HK, Choi CG, Suh DC, Lee KS, Khang SK. Malignant peripheral nerve sheath tumor in the parapharyngeal space: tumor spread through the eustachian tube. AJNR Am J Neuroradiol. 2001;22:748–50.
25. Ding JH, Hu CS, Peng WJ, Zhou ZR, Tang F, Mao J. Evaluation of MRI in nasopharyngeal carcinoma with cavernous sinus infiltration. Zhonghua Zhong Liu Za Zhi. 2006;28:530–2.
26. Sepehrnia A, Samii M, Tatagiba M. Management of intracavernous tumours: an 11-year experience. Acta Neurochir Suppl. 1991;53:122–6.
27. Spell DW, Gervais DS, Jr., Ellis JK, Vial RH. Cavernous sinus syndrome due to metastatic renal cell carcinoma. South Med J. 1998;91:576–9.
28. Nassiri F, Scheithauer BW, Corwin DJ, Kaplan HG, Mayberg M, Cusimano MD, Rotondo F, Kovacs K. Invasive thymoma metastatic to the cavernous sinus. Surg Neurol Int. 2013;4:74.
29. Pawakranond L, Laothamatas J. MRI findings of the cavernous sinus metastasis with inferior extension mimicking a nasopharyngeal carcinoma with cavernous sinus invasion. J Med Assoc Thai. 2006;89:890–5.
30. Erdem E, Angtuaco EC, Van Hemert R, Park JS, Al-Mefty O. Comprehensive review of intracranial chordoma. Radiographics. 2003;23:995–1009.
31. Goel A, Muzumdar DP, Nitta J. Surgery on lesions involving cavernous sinus. J Clin Neurosci. 2001;1:71–7.
32. Lanzino G, Sekhar LN, Hirsch WL, Sen CN, Pomonis S, Snyderman CH. Chondromas and chondrosarcomas involving the cavernous sinus: review of surgical treatment and outcomes in 31 patients. Surg Neurol. 1993;40:359–71.
33. Kim E. Fibrous dysplasia of the clivus. J Korean Neurosurg Soc. 2010;48:441–4.
34. Daffner RI, Kirks DR, Gehwciler JA, Jr., Heaston DK. Computed tomography of fibrous dysplasia. AJR Am J Roentgenol. 1982;139:943–6.
35. Ardehali MM, Samimi Ardestani SH, Yazdani N, Goodarzi H, Bastaninejad S. Endoscopic approach for excision of juvenile nasopharyngeal angiofibroma: complications and outcomes. Am J Otolaryngol. 2010;31:343–9.
36. Hirano H, Tashiro Y, Fujio S, Goto M, Arita K. Diffuse large B-cell lymphoma within a cavernous hemangioma of the cavernous sinus. Brain Tumor Pathol. 2011;28:353–8.
37. Arimoto H, Shirotani T, Nakau H, Hashizume K, Sakai Y, Matsukuma S. Primary malignant lymphoma of the cavernous sinus—case report. Neurol Med Chir (Tokyo). 2000;40:275–9.
38. Sadruddin S, Medeiros LJ, DeMonte F. Primary T-cell lymphoblastic lymphoma of the cavernous sinus. J Neurosurg Pediatr. 2010;5:94–7.
39. Han MH, Chang KH, Kim IO, Kim DK, Han MC. Non-Hodgkin lymphoma of the central skull base: MR manifestations. J Comput Assist Tomogr. 1993;17:567–71.
40. Gharabaghi A, Koerbel A, Samii A, Safavi-Abbasi S, Tatagiba M, Samii M. Epidermoid cysts of the cavernous sinus. Surg Neurol. 2005;64:428–33.
41. Tun K, Celikmez RC, Okutan O, Gurcan O, Beskonakli E. Dermoid tumour of the lateral wall of the cavernous sinus. J Clin Neurosci. 2008;15:820–3.
42. Miyajima Y, Oka H, Utsuki S, Kondo K, Sato K, Fujii K. Symptomatic Rathke's cleft cyst with cavernous sinus syndrome. Neurol Med Chir. 2007;47:576–8.
43. Linskey ME, Sekhar LN, Hirsch W, Jr., Yonas H, Horton JA. Aneurysms of the intracavernous carotid artery: clinical presentation, radiographic features, and pathogenesis. Neurosurgery. 1990;26:71–9.
44. Chapman PR, Gaddamanugu S, Bag AK, Roth NT, Vattoth S. Vascular lesions of the central skull base region. Semin Ultrasound CT MR. 2013;34:459–75.
45. Ellis JA, Goldstein H, Connolly ES, Jr., Meyers PM. Carotid-cavernous fistulas. Neurosurg Focus. 2012;32:E9.
46. Yoo K, Krisht AF. The cavernous sinus: a comprehensive text. 1st ed. Philadelphia: Lippincott Williams & Wilkins; 2000.
47. Barrow DL, Spector RH, Braun IF, Landman JA, Tindall SC, Tindall GT. Classification and treatment of spontaneous carotid-cavernous sinus fistulas. J Neurosurg. 1985;62:248–56.
48. de Keizer R. Carotid-cavernous and orbital arteriovenous fistulas: ocular features, diagnostic and hemodynamic considerations in relation to visual impairment and morbidity. Orbit. 2003;22:121–42.
49. Yamashita Y, Mitsuzaki K, Ogata I, Takahashi M, Hiai Y. Three-dimensional FISP imaging in the evaluation of carotid cavernous fistula: comparison with contrast-enhanced CT and spin-echo MR. J Magn Reson Imaging. 1998;8:1066–72.
50. Brismar G, Brismar J. Aseptic thrombosis of orbital veins and cavernous sinus. Clinical symptomatology. Acta Ophthalmol (Copenh). 1977;55:9–22.
51. Imholz B, Becker M, Lombardi T, Scolozzi P. Septic thrombosis of the cavernous sinus secondary to a *Streptococcus milleri* oral infection. Dentomaxillofac Radiol. 2012;41:525–8.
52. Schuknecht B, Simmen D, Yuksel C, Valavanis A. Tributary venosinus occlusion and septic cavernous sinus thrombosis: CT and MR findings. AJNR Am J Neuroradiol. 1998;19:617–26.
53. Rao KC, Knipp HC, Wagner EJ. Computed tomographic findings in cerebral sinus and venous thrombosis. Radiology. 1981;140:391–8.
54. Lee JH, Lee HK, Park JK, Choi CG, Suh DC. Cavernous sinus syndrome: clinical features and differential diagnosis with MR imaging. AJR Am J Roentgenol. 2003;181:583–90.
55. Tolosa E. Periarteritic lesions of the carotid siphon with clinical features of carotid intraclinoid aneurysms. J Neurol Neurosurg Psychiatry. 1954;17:300–2.
56. Hunt WE, Meagher JN, LeFever HE, Zeman W. Painful ophthalmoplegia: its relation to indolent inflammation of the cavernous sinus. Neurology. 1961;11:56–62.
57. Yousem DM, Atlas SW, Grossman RI, Sergott RC, Savino PJ, Bosley TM. MR imaging of Tolosa-Hunt syndrome. AJR Am J Roentgenol. 1990;154:167–70.
58. Schuknecht B, Sturm V, Huisman TA, Landau K. Tolosa-Hunt syndrome: MR imaging features in 15 patients with 20 episodes of painful ophthalmoplegia. Eur J Radiol. 2009;69:445–53.
59. Wasmeier C, Pfadenhauer K, Rosler A. Idiopathic inflammatory pseudotumorof the orbit and Tolosa-Hunt syndrome: are they the same disease? J Neurol. 2002;249:1237–41.
60. Kim JH, Chang KH, Na DG, Park SH, Kim E, Han DH, Kwon HM, Sohn CH, Yim YJ. Imaging features of meningeal inflammatory myofibroblastic tumor. AJNR Am J Neuroradiol. 2009;30:1261–7.
61. Miwa H, Koshimura I, Mizuno Y. Recurrent cranial neuropathy as a clinical presentation of idiopathic inflammation of the dura mater: a possible relationship to Tolosa-Hunt syndrome and cranial pachymeningitis. J Neurol Sci. 1998;154:101–5.

62. Wild T, Strotzer M, Volk M, Feuerbach S. Idiopathic hypertrophic cranial pachymeningitis associated with an orbital pseudotumor. Eur Radiol. 1999;9:1401–3.
63. McKinney AM, Short J, Lucato L, SantaCruz K, McKinney Z, Kim Y. Inflammatory myofibroblastic tumor of the orbit with associated enhancement of the meninges and multiple cranial nerves. AJNR Am J Neuroradiol. 2006;27:2217–20.
64. Toyoda K, Oba H, Kutomi K, Furui S, Oohara A, Mori H, Sakurai K, Tsuchiya K, Kan S, Numaguchi Y. MR imaging of IgG4-related disease in the head and neck and brain. AJNR Am J Neuroradiol. 2012;33:2136–9.
65. Kubota T, Moritani S. Orbital IgG4-related disease: clinical features and diagnosis. ISRN Rheumatol. 2012;2012:412896.
66. Reynaud Q, Palaghiu D, Barral FG, Camdessanché JP, Cathébras P. An ANCA negative limited form of granulomatosis with polyangiitis (Wegener's granulomatosis) affecting the cavernous sinus. Rev Med Interne. 2013;34:237–41.
67. Zarei M, Anderson JR, Higgins JN, Manford MR. Cavernous sinus syndrome as the only manifestation of sarcoidosis. J Postgrad Med. 2002;48:119–21.
68. Jaimovich SG, Thea VC, Guevara M, Gardella JL. Cavernous sinus tuberculoma mimicking a neoplasm: case report, literature review, and diagnostic and treatment suggestions for tuberculomas in rare locations. Surg Neurol Int. 2013;4:158.
69. Boutarbouch M, Arkha Y, Gana R, El Maquili MR, Bellakhdar F. Tuberculoma of the cavernous sinus mimicking a meningioma: case report and review of the literature. J Neurol Sci. 2009;278:123–6.